For Submission to Journal of Geophysical Research: Earth Surface
Preprint date: March 10, 2022

Salt Marsh Response to Increased Tidal Inundation

Authors:
Yellen, B.[1], Woodruff, J.D.[1], Baranes, H.E.[1], Geyer, R.[2], Engelhart, S.E.[3], Randall, N.[4], Griswold, F[1].

[1]University of Massachusetts Amherst, [2]Woods Hole Oceanographic Institution, [3]Durham University, [4]U.S. Geological Survey

Key Points:

- A change in inlet location and resultant tidal channel shortening caused an immediate increase in effective sea level and marsh inundation
- Increased salt marsh inundation drove early 20th century deposition rates that were roughly three times the rate of relative sea level rise
- Deposition rates increase with proximity to the new inlet
- Minerogenic sediment deposition is critical to marsh survival under rapid rates of sea level rise

Abstract

Barrier inlets and marshes behind them are often viewed and managed as separate systems with independent controls because they are affected by different boundary conditions. Here, we make use of a 120-year-old storm-driven change in inlet location to illustrate how barrier beaches and wetland processes are intricately linked. Further, we show that tidal marshes can be resilient to a rapid increase in inundation given sufficient sediment supply and discuss implications for coastal management along sediment-deficient coastlines.

In 1898, a coastal storm eroded a new inlet through the barrier beach that fronts the North-South Rivers Estuary in Massachusetts, USA. The old inlet silted in after the storm, and the change in inlet location shortened the North River channel by 5.6 km. After the inlet location change, historical records indicated increased high tide levels along the North River. We make use of this increase in water levels and associated marsh response to examine conditions that have allowed for marsh resilience after a rapid increase in inundation depth. Sediment cores show that increased mineral sediment deposition after 1898 played a dominant role in allowing marshes along the North River channel to adjust to greater inundation. To accommodate greater tidal flow after the change in inlet location, the North River channel widened by an

average of 18%. Edge erosion from channel widening likely provided sediment to the marsh platform. Modern water level monitoring along the channel shows that mean high water declines landward by at 4.8 cm/km up to 10 km from the inlet. North River channel shortening thereby likely increased mean high water by at least 27 cm within the lower estuary. At present, the marsh platform elevation along both channels has largely reequilibrated to the effective change in sea level, with similar marsh inundation depths along both channels of the estuary. The role of mineral sediment in allowing for rapid marsh sediment deposition and resilience of this marsh to an abrupt increase in inundation depth points to the importance of management strategies that maintain sediment supplies to coastal regions.

1. Introduction:

Salt marshes aggrade in quasi-equilibrium with sea level rise via the accumulation of organic matter and mineral sediment, thereby maintaining marsh platform elevation within the tidal frame (Allen, 2000; Cahoon et al., 2019). External perturbations, such as an acceleration in relative sea level rise (SLR), can be compensated for by two main mechanisms. First, the resultant increase in inundation depth tends to augment sediment delivery to the marsh platform as the flood duration and time to trap suspended sediment increases (Day et al., 1999; Reed, 1990; Temmerman et al., 2003). Second, bioproductivity and belowground biomass production tend to increase with increasing inundation depth up to a threshold where marsh grasses die (Pomeroy et al., 1981; Snedden et al., 2015). Under moderate rates of relative SLR, marshes can persist for thousands of years by building vertically (Pederson et al., 2005; Redfield, 1972) and/or transgressing into uplands (Rampino and Sanders, 1980). However, submerged salt marsh peat found far offshore dating to the early Holocene (Emery et al., 1965; Wolters et al., 2010), when global SLR rates were ~10-15 times higher than rates over the last 6000 years (e.g., Lambeck et al., 2014), indicates that marshes fail when SLR exceeds their ability to build elevation or when SLR-driven shoreline transgression removes the protective morphologies (e.g. barrier beaches) that enable marsh development. Many studies have modeled SLR rate thresholds for marsh survival under various projections of future SLR using known relationships between marsh inundation, sediment supply, and observed vegetative response to changing inundation depth (D’Alpaos et al., 2007; French, 2006; Kirwan and Guntenspergen, 2010; Langston et al., 2020). However, these studies can only be performed in model space, as physical experiments testing the effect of rapidly rising sea level on tidal marsh resilience would be impractical and prohibitively expensive.

While it is impossible to directly observe how salt marshes will respond to sustained accelerated SLR in the future, we can make use of past instances of rapid increases in tidal inundation to inform our understanding of factors that improve marsh resilience to SLR. Several examples exist of changes in tidal dynamics or land elevation leading to rapid, local increase in tidal inundation and impacts to marshes. Removal of tidal restrictions such as undersized culverts can increase the height of high tide and the resulting tidal inundation of the marsh platform. Boumans et al. (2002) point out that removal of tidal restrictions should be done with care, as the rapid increase in inundation could further stress degraded marshes, especially those that subsided while tides were restricted. Tectonic events that result in coastal subsidence can quickly increase sea level relative to tidal marsh elevation. At many estuaries adjacent to the Cascadia Subduction Zone (northern California, Oregon, and Washington USA; British Columbia, Canada), sediment records provide evidence for repeated transitions of salt marsh to intertidal mudflat following earthquakes that increased relative sea level in excess of 0.5 m (e.g., Atwater and Hemphill-Haley, 1996). Subsequent reestablishment of the marsh is recorded in the sedimentary record as couplets, with mineral rich sediment overlying organic rich soils or peats that grade back into organic salt marsh sediments (Shennan et al., 1996). Rapid seismically-induced subsidence along active margins is typically followed by uplift that reduces the rate of relative SLR once the tectonic plates become coupled again. While the role of tectonics in driving changes to relative sea level and marsh response has been well documented, marsh impacts from changing barrier/inlet dynamics and resultant tidal adjustments are less certain. On passive margins, where salt marshes are more common, barrier/inlet dynamics may play a first order role in mediating tidal propagation and impacts to salt marshes.

Connections between barrier dynamics and lagoonal tidal wetlands have long been established. Landward of barrier island complexes, Lucke (1934) highlighted the tendency for tidal marshes to initiate on flood-tide deltas. Barrier inlet stability plays a first order control on the subsequent development and morphology of back barrier marsh complexes, with divergent marsh geometries forming behind stable versus migrating barrier inlets. Migration of inlet locations can affect tidal marsh sedimentation rates, with increased proximity of marine sediment driving enhanced delivery of mineral sediment (Roman et al., 1997). The spacing between tidal inlets is controlled in large part by tidal range, with larger tidal prisms requiring more closely spaced inlets (FitzGerald, 1988; Hayes, 1979), which in turn can control where marshes initiate within lagoons. However, the impact of abrupt changes in inlet location on back barrier marshes is relatively understudied despite the relatively frequent nature of barrier breaches leading to new inlet formation.

Here we make use of an historic change in tidal inlet location to the North-South Rivers Estuary, first to illustrate how the estuary’s tidal marsh responded to resultant increased tidal elevations, and second to show the role of inlet location in controlling tidal propagation up estuarine channels. To our knowledge, this is the first study to highlight the first order control of inlet location on tidal heights and salt marsh response. Results from this study can help guide tidal marsh restoration involving the removal of tidal restrictions and encourage coastal management practices that treat sediment as a valued resource.

2. Site Description

2.1 North-South Rivers Estuary

Our study site, the North-South Rivers Estuary (NSRE) is a mesotidal (~3.5 m tidal range) bar-built estuary with two main channels, the 20 km North River and 13 km South River, which are connected to Massachusetts Bay by a shared inlet (Fig. 1). Channel widths are approximately 100 meters within their seaward reaches and narrow continuously up-estuary to ~30 m and ~15 m at the head of tides on the North and South Rivers respectively. Both tidal channels are fringed by a high marsh platform that is generally 300-500 m in width. Low marsh areas are largely confined to channel proximal areas less than 2 km from the new inlet (Fig. 1), where the estuary has more of an open embayment morphology rather than a confined channel. Previous work investigating the timing of turbidity increases within the North and South Rivers and sediment deposition on the marsh platform showed that marine sediment delivered on the flood tide during coastal storms provides the primary source of suspended sediment to the estuary and marsh (Baranes et al., 2022). Sediment inputs from the watersheds of the North River (area = 210 km^2) and South River (area = 60 km^2) are relatively minor.

Relative SLR at the Boston tide gauge, 35 km north along the coast, has averaged 2.87 +/- 0.15 mm/yr during 1920-2020 (NOAA gauge 8443970). Tidal range in Massachusetts Bay averages about 3 m, similar to that observed at mouth of the North-South Rivers Estuary (Buynevich and Donnelly, 2006), with that range decreasing up-estuary (Roman et al., 1997; Baranes et al., 2022). Salt marsh accumulation rates for the last 100 years, constrained by continuous radiometric dating of ten cores located just south of our study location in Cape Cod Bay, averaged 3.9 mm/yr, with a range 2.7 to 5.2 mm/yr (O'Keefe Suttles et al., 2021).

2.2 The Portland Gale and Recent History

In 1898, waves and storm surge from the Portland Gale eroded a new cut through the barrier beach that shelters the NSRE~~estuary~~. The old, more southerly inlet closed by 1900 (Frietas and Ball, 1995), with the new northern inlet resulting in a 5.6 km shortening of the North River channel and equal lengthening of the South River (Fig. 1) (Buynevich and Donnelly, 2006). Firsthand accounts of the storm's aftermath noted increased frequency of high marsh flooding along the North River after the inlet switch (Freitas and Ball, 1995).

Industrial pollution has also left its mark on the estuary. A former munitions manufacturing, testing, and disposal facility called “The Fireworks Site” is located on a tributary to the North River in Hanover, MA (Fig. 1). The facility began operations during World War I (1914-1918) and is known to have used lead and mercury in its manufacturing processes (Town of Hanover, 2008), which have since been found in high concentrations in surrounding surface water, sediment, and fish tissue (Tetra Tech, 2005)

We make use of this natural experiment of an abrupt change in inlet location and channel shortening to observe resultant impacts to tidal heights and salt marsh inundation along the North River. We combine water column observations, elevation surveys, and sediment cores to evaluate what conditions allowed the estuary’s marsh to survive this stressor. Observations from these systems can provide useful guidance for coastal preparedness and conditions that may allow marshes to survive projected near-term SLR acceleration.

3. Methods:

3.1 Sediment cores and probing

We collected 1 m sediment cores during March of 2018 from six locations on the marsh platform along the North River channel (N1-N6) and four locations along the South River channel (S1-S4) (see Fig. 1 for locations). We used a 6 cm internal diameter gouge corer, which results in negligible vertical compaction and allows for visual observation in the field (Yellen et al., 2021). Core transects at each site extended away from the tidal river channel so that we could characterize changes in lithology and deposition rate with increasing distance from the channel. During low tide conditions, we observed a visually distinct stratum within the North River channel banks approximately 60-80 cm below the marsh platform that was characterized by erosion-resistance (protruding past other layers) and a reddish color. Within marsh gauge cores, this stratum was also easily visually identified away from the channel. We used field observations of the depth to this layer in cores from the North River marsh as a chronostratigraphic tie point to assess relative deposition rates. We refer to this layer within this paper as the “marker horizon.” No such layer was observed in South River cores or along South River exposed channel banks.

3.2 Sediment processing

Sediment cores were processed to identify temporal and spatial variability in deposition rate and sediment composition within the NSRE~~North and South Rivers system~~. Sediment cores were transported to the University of Massachusetts, where they were split, described, and evaluated for down-core elemental abundances via X-ray fluorescence (XRF) core scanning (Croudace et al., 2006). A clear onset of elevated heavy metals evident in the XRF-derived bulk lead profile was used to assess relative sedimentation rates in South River marsh sites where the organic marker horizon was absent. The bulk lead onset depth is associated with the timing of industrialization, and generally dates to the late 1800s in this region (Nixon, 1995). Lead XRF counts were converted to concentrations according to an empirical regression based on North and South River marsh cores from Baranes et al. (2022).

We used radiometric dating via down-core ^{137}Cs and ^{210}Pb profiles to constrain the date of the increase in bulk lead (Anisfeld et al., 1999; Cundy and Croudace, 1996). We chose representative cores N3C1 and S3C3 for gamma spectroscopy from transects N3 and S3 based on the following criteria: the core had to be a minimum of 20 m from the channel to avoid creek edge impacts that include lateral erosion, levying, and subsidence (Roner et al., 2016); the core top elevation was roughly equivalent to median marsh platform elevation; and the core's XRF-derived bulk lead profile enabled identification of the onset and peak of industrial metal contamination (Supp. Fig 1). Age versus depth models were obtained based on the depletion of ^{210}Pb in core subsamples via the constant rate of supply model (Appleby and Oldfield, 1978) and the 1954 CE onset and 1963 CE peak in ^{137}Cs concentrations (Pennington et al., 1973).

We subsampled 1 cm depth intervals from sediment cores every 10 cm to assess soil organic matter via loss on ignition (LOI), combusting dried and weighed samples at 550 °C for four hours (Dean, 1974). We increased sample resolution in representative cores S3C3 and N3C1 above and below the organic marker horizon in all North River marsh cores and surrounding bulk lead onset depths in South River cores.

3.3 Foraminifera

Foraminiferal assemblages can be used to assess environmental conditions indicative of marsh inundation frequency (e.g., Scott and Medioli, 1978). Foraminifera were processed from core N3C1 according to standard methods (Scott and Medioli, 1980) and summarized here. Core subsamples spanning 1 cm from above and below the organic marker horizon were washed through sieves to isolate the 63-500 micron fraction and counted wet under a binocular microscope. The greater than 500-micron fraction was checked for larger foraminifera. A minimum of 50 individuals were counted in each sample to ensure that it accurately characterized the assemblage (Kemp et al., 2020). Our taxonomy follows Wright et al. (2011) and references therein.

3.4 Water surface elevation

In order to assess the elevation of the marsh platform relative to the tidal frame, water surface elevation was measured at N1-N6 and S1-S4 (Fig. 1). Continuously logging pressure transducers were mounted to rebar and deployed in the channel below the lowest low tide level at each location and surveyed to NAVD88 with Real Time Kinematic GPS (RTK). Observations from a subaerial pressure transducer were used to correct water levels for barometric effects. Continuous salinity and temperature measurements adjacent to each pressure transducer were used to correct for density variations. Data loggers collected data for 40 days and therefore captured spring-neap tidal variability. We computed a 1983-2001 National Tidal Datum Epoch equivalent MHW datum at each sensor location using the NOAA Tidal Analysis Datums Calculator with the Boston NOAA gauge as a control station.

3.5 Marsh surveying and channel dimensions

We surveyed marsh platform elevation with RTK GPS along transects perpendicular to the channel edge at water level monitoring sites during March of 2018. Average elevation sample size was 65 points, with an average horizontal and vertical accuracy of 2 cm. All sites were characterized by high marsh grass species *Spartina patens* and short form *Spartina alterniflora* (Bertness, 1991), except for site N1, which is low marsh and dominated by tall and short form *S. alterniflora*.

We compared mapped channel widths from before and after the 1898 inlet location change to evaluate changes in channel dimensions as a result of the inlet switch. We georeferenced a detailed 1870 map of the North-South Rivers Estuary (Peirce et al., 1870) that clearly depicted the marsh edge to make pre-1898 channel measurements. In a geographic information system, channel widths were measured every 0.25 km along both estuarine channels, with channel width defined as marsh edge to marsh edge. The same measurements were made on a georeferenced 2019 orthomosaic aerial photo (MassGIS, 2019). North River width measurements began 3 km from the new inlet where the estuary transitions from an open embayment morphology to a confined channel, and continue up to the head of tides (river km

20). South River measurements span river km 6.5 to 10, beginning at the old inlet location, and ending at the edge of the 1870 map coverage.

4. Results:

4.1 Deposition Rates, Stratigraphy, and Foraminifera

We used short lived radionuclides to constrain the deposition rates of representative marsh cores from the North River and South River marshes. Age models based on ^{210}Pb and ^{137}Cs from these representative cores indicated roughly twice as much deposition at N3 than at S3 since ~1900 (Fig. 2A). The average deposition rate in the upper 72 cm of the North River core (since ~1900) was 6.1 mm/yr. South River deposition during the same period at S3C3 averaged 3.0 mm/yr.

Bulk lead concentrations and organic content (LOI) profiles are shown in Figure 2B to relate the dates of the heavy metal contamination onset and organic marker horizon to the age model. At transect N3, the depth of the organic marker horizon (see section 3.1) is clearly depicted by high LOI values between 67 and 70 cm and is contemporaneous with the step function rise in bulk lead contamination. LOI values decreased to 7% immediately above the marker horizon, and then slowly increased towards the surface. This indicates an increase in clastic content above the marker horizon, followed by a gradual increase in organic content toward present. In contrast to N3, LOI at S3 increased above background levels following the increase in bulk lead and remained elevated to the present, indicating persistent increase in organics after the early-1900s. .

A comparison of the onset depth of lead contamination across the estuary indicated generally higher 20th century accumulation rates along the North River marsh than in the South River marsh, consistent with observations from our cores dated via gamma spectroscopy (Fig. 3). While Figure 2 depicts lead profiles from a single representative core from each marsh transect, depositional patterns were consistent across marsh transects (Supp. Fig. 1). At up-estuary North River transects (N4-N6), the sediment thickness above the base of lead contamination totaled approximately 60 cm versus 40 cm depth at S2-S4, indicating ~50% more accumulation since industrialization. At cores N1-N3 and S1, located closer to the new inlet that formed in 1898, lead onset depth increased with proximity to the new inlet, with approximately 122 cm of sediment deposition at site N1 since the initial rise in lead abundance. Baranes et al. (2022)

noted a marked up-estuary increase in sediment lead abundance along the North River (note that the x-axes change in Fig. 3), much of which was sourced from an upstream contaminated site (Tetra Tech, 2005). Down-estuary lead dilution provided evidence for a dominant marine sediment source to the estuary (Baranes et al., 2022).

Foraminiferal assemblages were enumerated from core N3C1 (Fig. 4) to assess changes in tidal inundation depth and frequency associated with the organic marker horizon at 67-70 cm depth. The two foraminiferal samples below the organic horizon (70-71cm and 75-76 cm) were characterized by an assemblage dominated by high marsh species. In contrast, samples from 65-66 cm and 60-61 cm reflected lower marsh conditions with more frequent flooding. Specifically, samples below the organic horizon included *Jadammina macrescens* and *Trochammina inflata* (96-98%, respectively) with <1% of species including *Miliammina fusca*, *Ammobaculites* spp, and *Reophax* spp. At 65-66 cm, there was a switch in assemblage to species more associated with more frequent tidal inundation. *M. fusca (9%)*, *Ammobaculties* spp (9%), and *Reophax* spp. (<1%) to 19% of the assemblage while continuing to be dominated by J. macrescens (75%). This pattern continues at 60-61 cm with an increase in *M. fusca (50%)* and *Ammobaculites* spp. (30%) to 80% of the assemblage with *J. macrescens* significantly reduced (6%). This trend continues up core at 45-46 cm with increasing *M. fusca* (70%), *J. macrescens* (20%), and *T. inflata* (7%) and a reduction in *Ammobaculites* spp (1%). Towards the top of the core at 15-16 cm, there is a reduction in *M. fusca* (61%) and *J. macrescens* (13%) and an increase in *T. inflata* (21%) and *Tiphotrocha comprimata* (5%).

4.2 Along Channel Tidal Observations

MHW elevation generally decreased with increasing distance from the inlet, with roughly equal tidal attenuation observed in the North and South River channels. MHW ranged from a maximum 1.50 m NAVD88 near the inlet (location N1) to a minimum of 1.12 m NAVD88 on the South River at S4 (12.2 km from the inlet) and a minimum of 1.19 m NAVD88 on the North River at N5 (12.8 km from the inlet; Fig. 2A). MHW elevation decreased 4.8 cm per km up-estuary from the inlet along both estuarine channels up to 8.5 km from the shared inlet. This trend reversed in the upper reaches of the North River tidal channel, with MHW elevation increasing by 5 cm over the 3.5 km from N5 to N6 (Fig. 2B). For seaward sites (less than 8.5 km from the inlet), MHW elevation was approximately 5 cm higher in the North River channel than in the South River at equivalent distances from the inlet, with the difference decreasing to zero at distances more than 12 km from the inlet (Fig. 2A).

4.3 Marsh Platform Elevation

Median marsh platform elevation along the North River channel tended to decrease up-estuary (Fig. 5). Site N1, a low marsh site exposed to wave energy from the inlet, was an exception. Along the South River, median marsh elevation increased from sites S1 to S3 and decreased towards S4 (Fig. 5A). Marsh platform 25th-75th centile elevations varied less than 10 cm within individual transects at each site (again with the exception of N1). The average 25th-75th centile elevation range at sites N2, N3 and S1-S4 was 5 cm. At upper estuary sites N4-N6, marsh elevation varied even less, averaging 3 cm for the same metric.

We estimated average marsh inundation depth at high tide throughout the estuary by subtracting median marsh elevation from MHW values at each transect. Marsh inundation depth generally decreased up-estuary, ranging from 0.81 m at the mouth (site N1) to 0.25 m at S3 and S4 (Fig 5B). Inundation depths on the South River marsh were less than those on the North River at all equivalent distances from the inlet except S1, which is located between the old and new inlet locations, and therefore did not experience channel shortening as result of the inlet switch. High-marsh average inundation depths in the lower estuary (< 8 km from the inlet) were 0.47 m on the North River (N2-N4) and 0.42 m on the South River (S1-S3). In the upper estuary, (N5, N6, S4), North River marsh inundation averaged 0.46 m, which was nearly double the inundation depth of 0.25 m along the upper reaches of the South River (Site S4).

4.4 Marsh channel dimensions

Channel width measurements from 1870 and 2019 indicated a coherent signal of channel widening along the North River, but not the South River (Fig. 6). North river channel width measurements indicated an average increase of 18% (standard error = 3%) across the 49 measured locations, with 32 of the locations experiencing > 10% widening, and only four experiencing > 10% narrowing. Conversely, the South River did not experience widening. Depiction of the South River on the 1870 map extended upstream only to river km 10.5, and therefore only allowed for 16 width measurements. Of the 16 width change observations, five showed widening and three showed narrowing of more than 10%, with an average widening of 4% (standard error = 3%). The widening of the North River channel represents horizontal erosion of the marsh platform. Using the reach lengths, change in channel width, and an average bank height of 3 m, we estimated the total eroded volume of marsh soil equaled 330,000 m^3. If this sediment were redistributed equally across the entire area of the present-day

North River marsh platform assuming a similar bulk density of the eroded and deposited material, it would account for 6-8 cm of deposition.

5. Discussion:

5.1 Marsh accumulation rates and stratigraphy

Based on the timing and stratigraphy surrounding the cohesive, organic-rich marker horizon evident at transects N1-N4, we interpret the layer as a pre-1898 stable high marsh platform. The transition from foraminifera assemblages at N3 dominated by *J. macrescens* and *T. inflata* (below 70 cm depth) to an assemblage with increased *M. fusca*, *Ammobaculites* spp. and *Reophax* spp. (shallower than 65 cm depth) is consistent with this part of the North River marsh transitioning to experiencing greater inundation after 1898. Specifically, the change in foraminifera assemblage suggests a change in depositional environment from at or above MHW before the inlet switch to below MHW afterward. Following the inlet switch and resultant increase in MHW along the North River, sediment organic content abruptly decreased from 46% to 7% at our representative N3 transect core (Fig. 2A). The mineral-rich nature of this overlying sediment reflects a greater hydroperiod and inundation depth following the inlet switch (Temmerman et al., 2003).

Sediment accumulation rates over the first half of the 20th century (1898-1963) of 5.8 mm/yr were nearly four times the regional rate of SLR during that time (Talke et al., 2018). Furthermore, accumulation rates during the first 1-2 decades after the inlet switch (i.e. 1900-1920) were likely higher, but radionuclide data do not allow for resolution of shorter term accumulation rates. Rapid accumulation rates in the early 1900s were initially supported largely through enhanced trapping of mineral sediment. As the marsh built elevation over the ensuing decades, inundation depths and mineral sediment trapping decreased, which is reflected by the increase in LOI towards the core top. Sedimentation rates remained high from 1963 to the present, averaging 6.3 mm/y; however, this is only twice the rate of SLR over the same time period of 3.0 mm/yr, and therefore reflects a deceleration relative to the rate of SLR. Proximal to the new inlet, at sites N1 and N2, sediment accumulation rates since the inlet switch were even greater (10.1 and 7.5 mm/yr respectively based on a ~1900 date for bulk lead onset). For reference, the average accumulation rate for the last ~100 years at ten other Massachusetts Bay marshes with well-constrained age models was only 3.9 mm/yr (SD=0.75 mm/yr), or 1.35 times the rate of SLR, with a maximum reported accumulation rate of 5.2 mm/yr (O'Keefe

Suttles et al., 2021). Our most recently sampled foraminiferal assemblages at 15-16 cm (~CE 1990) contain significant *M. fusca*, which shows that the marsh had yet to reach the same inundation frequencies as prior to the inlet switch. This suggests a recovery period in excess of ~90 years.

The North River marsh's high accumulation rates provide an example of how a salt marsh can adjust to greater inundation depths when there is a sufficient external sediment supply. In general, the NSRE is a mineral rich system, with a mean LOI of 24% in the upper 50 cm of the marsh platform across core transects less than 12 km from the inlet. For reference, the mean LOI value from the upper 50 cm of 99 sediment cores from the Northeast US evaluated by Holmquist et al. (2018) equals 38%. At nearby Nauset Marsh (Cape Cod, Massachusetts, USA), sedimentation rates of up to 23.7 mm/y of largely mineral material were observed in response to the system's inlet migrating toward the measurement location. These rates were more than ten times higher than those observed far from the inlet. Were high temporal resolution observations available for the North River marsh in the early 1900s, we would expect similarly high accumulation rates immediately following the inlet switch.

Marshes along the South River channel were also affected by the inlet switch and resultant adjustment in water levels. Unlike the North River, South River MHW likely decreased in response to the inlet switch lengthening its channel by 5.6 km and nearly doubling the length of its tidal reach. Based on present day MHW attenuation of 4.8 cm/km, marsh inundation depths likely decreased by roughly 27 cm after the old inlet closed completely. The observed increase in LOI above the bulk lead onset, which we interpret as roughly coincident with the inlet switch, is consistent with decreased inundation in the South River marsh resulting in less sediment trapping and a shift towards more organogenic conditions. South River marsh accumulation rates at S3 of 3.0 mm/yr during the last 100 years were slower than nine out of ten reported marsh accumulation rates from the region (O'Keefe Suttles et al., 2021). The relatively slow sediment accumulation rates observed for the South River are likely due mostly to reduced inundation depth and hydroperiod, which would have limited mineral material deposition (Temmerman et al., 2003) and suppressed bioproductivity (Mudd et al., 2009). Furthermore, lengthening of the South River channel due to the closing of the old inlet would have decreased delivery of marine sediment, the system's primary mineral sediment source (Baranes et al., 2022). The decrease in MHW may also have led to more oxidizing conditions within the marsh soil. Tidal restrictions that similarly decrease MHW have been observed to cause peat collapse and aerobic oxidation of soil organic matter that lead to subsidence (Anisfeld et al., 1999). If the decrease in South River MHW following the inlet switch led to marsh peat oxidation and subsidence, tides may have been able to inundate the marsh along the upper section of its tidal reach.

The Morris (2007) marsh equilibrium model can provide context for how North River marshes were able to persist following the increase in inundation depths caused by the 1898 inlet switch. The model predicts that marsh elevation change varies proportionally to inundation depth and biomass production. Inundation also controls biomass production, which Morris fit to a negative parabolic relationship such that biomass production increases at greater inundation depth, but collapses above some threshold depth at which the marsh drowns. Given NSRE's tidal range, biomass production would likely peak at around 1 m inundation depth, and collapse at around 2 m (Kirwan and Guntenspergen, 2010). Thus, both increased mineral sedimentation and biomass production likely contributed to North River marsh persistence following the 1898 increase in MHW.

Allen (1997) interpreted silt-peat transitions in marsh sediment as largely the product of local engineering projects or large-scale forcing such as changes in SLR or seismically-induced subsidence. Here we show that inlet dynamics that affect the propagation of tides may cause similar changes in lithology through stratigraphic sections. Presently marsh elevations relative to MHW are similar along the North and South Rivers at corresponding distances from the inlet, suggesting that the system has moved towards equilibrium with respect to the 1898 disturbance (Fig. 5). Increased mineral sediment accumulation following the inlet switch was likely in part due to increased hydroperiod (Allen, 2000; Temmerman et al., 2003), but it is also likely that sediment concentrations increased in the North River after the inlet switch. The opening of the new inlet through the beach between two prominent bluffs comprised of glacial till (Baranes et al., 2022) exposed these deposits to enhanced erosion that likely supplied fine grained mineral material to the North River marsh. Furthermore, the increased tidal prism within the North River channel network caused by the increase in MHW widened its channel, with eroded bank material providing an additional source of sediment. The mixed foraminiferal assemblage of low and high marsh foraminifera found immediately above the cohesive high marsh sediment supports rapid bank erosion as a source of sediment to the marsh platform, which has been documented in the region (Hopkinson et al., 2018).

5.2 Tidal elevations and marsh morphology

Modern MHW elevations decrease up-estuary at similar rates within the two main channels of the estuary, suggesting that the balance between channel friction and inertial forces within this system is roughly equivalent between the two main channels. This balance between dissipative and momentum forces in convergent estuarine channels, defined as those whose width decrease in the landward direction, is well documented in theoretical discussion (Fagherazzi and Furbish, 2001; Green, 1838; Jay, 1991; Lanzoni and Seminara, 1998). Our observations of decreasing landward MHW provide an example of a moderately dissipative system, with a slight increase in MHW at our most landward site N6 caused by wave reflection off the head of the estuary.

Historical maps as far back as 1870 (Gannett and Grambs, 1888; Peirce et al., 1870) indicate that channel locations have been relatively stable with the exception of the inlet switch. Aerial imagery from 1951 (University of Massachusetts, 1951) confirms stable channel dimensions since the mid-20th century. We therefore assume that pre-1898 up-estuary MHW attenuation occurred at a similar rate. Based on this assumption, the 5.6 km shortening of the North River channel would have caused a MHW increase of roughly 27 cm, which is equivalent to present day total inundation depths at site S3 and S4. Firsthand accounts support this interpretation of an instantaneous increase in MHW along the North River. For example, *S. alterniflora* replaced *S. patens* along North River marshes, and the North River Boat Club house (river km 6.5) had to be moved due to regular flooding immediately following the inlet switch (Freitas and Ball, 1995). Furthermore, an Atlantic white cedar stand located just upstream of N5 (42.112714, -70.779918) died following the inlet switch, consistent with higher water levels drowning these trees (F. Freitas, personal communication, 2021). The platform morphology of the estuary's marshes, which is common to this region (FitzGerald and Hughes, 2019), dictates that any change in tidal propagation over the marsh will have a disproportionate impact on tidal prism volume and resultant tidal velocities. North River marshes comprise roughly two thirds of the total estuarine area, and therefore, the increase in North River marsh inundation would have dramatically increased the tidal prism. We attribute the increase in North River channel widths (Fig. 6) to this increase in tidal prism.

5.3 Implications for Marsh Resilience

Observations presented here have implications for both beach and marsh management. With respect to beaches, we illustrate that inlet location can be a first order control in modulating local tidal heights, with the MHW increase from inlet switch equaling or exceeding the magnitude of relative SLR at this location for the preceding century. Therefore, in mesotidal systems, variations in tidal range caused by dredging (e.g., Ralston et al., 2019), changes in inlet location, or channel straightening, can have larger short term impacts on marshes than SLR. With respect to marshes, the 1898 rapid increase in North River MHW provides an example of greater inundation allowing for enhanced biomass production (Morris, 2007) and increased delivery of mineral sediment (Mudd et al., 2009; Temmerman et al., 2003). It is likely that generally high sediment loads from coastal erosion of fine-grained glacial deposits following the inlet switch in part allowed for this rapid adjustment, which perhaps cannot be counted upon across settings. If marshes are to survive rapid SLR, especially in sediment-deficient regions like the Northeast US, we need to assure that marshes have continued access to mineral sediment supplies. Dredging that removes sediment from the system presents an added stressor (Chant et al., 2021) that compounds the effects of accelerating SLR and eutrophication (Deegan et al., 2012; Turner et al., 2009; Watson et al., 2014). Engineering of the coastline to halt erosion may have the unintended consequence of reducing sources of sediment important to marsh health (Baranes et al., 2022). In coastal regions that lack large supplies of suspended fluvial sediment, such as the Northeast US and the Maritimes of Canada, managers must consider alternate supplies of sediment to replace the potentially reduced sediment flux from armored coastlines and dredging projects.

In addition to abundant sediment supplies provided in part by glacial legacy sediments at the new inlet, marsh systems that formed behind barrier beach systems depend on the stability of the beach location to persist. The NSRE barrier beach is anchored in part by erosion-resistant headlands (drumlins) that help to stabilize the beach location. Where steep uplands prevent substantial landward marsh migration, marsh vertical accretion can play a dominant role in marsh persistence, but only if an external suspended sediment supply is maintained.

Conclusion

A change in inlet location to the North-South Rivers Estuary during the 1898 Portland Gale caused an abrupt ~27 cm increase in mean high water along the shortened North River, illustrating the role of barrier dynamics in modulating tidal inundation depths in salt marshes. The increase in tidal heights provided an opportunity to observe resultant changes to tidal marsh lithology and elevation under conditions analogous to rapid sea level rise. North River tidal marshes proved resilient to increased inundation, rapidly building elevation at up to five times the rate of regional SLR over the same time period and have moved towards equilibration with the step change in tidal inundation depths. Initially, rapid accumulation of inorganic material played a large role in building elevation, providing evidence that mesotidal marshes with sufficient supplies of mineral sediment should be resilient to projected future sea level rise. Dredging and shoreline armoring currently reduce marine sediment, the main supply of sediment in the Northeast US, where rivers supply limited amounts of sediment. Therefore, in order to build tidal marsh resilience, management efforts should be focused on creative solutions to restoring sediment sources lost when dredging and shoreline armoring are unavoidable.

Acknowledgements

The project described in this publication was in part supported by Grant or Cooperative Agreement No. G20AC00071 from the U.S. Geological Survey and a Department of Interior Northeast Climate Adaptation Science Center graduate fellowship awarded to H.E.B and B.C.Y. (G12AC00001). Its contents are solely the responsibility of the authors and do not necessarily represent views of the Northeast Climate Adaptation Science Center or the USGS. J.D.W. did initial analyses for this publication while in residency at the Darling Marine Center. David Ball and Fred Frietas of Scituate, MA provided useful guidance on firsthand accounts of the 1898 Portland Gale.

Data availability statement

The NOAA Tidal Analysis Datums Calculator software is available here: https://access.co-ops.nos.noaa.gov/datumcalc/CalculateDatums. Tidal marsh and channel observations are available here: https://orcid.org/0000-0002-1576-5220.

Citations

Allen, J.R.L., 2000. Morphodynamics of Holocene salt marshes: a review sketch from the Atlantic and Southern North Sea coasts of Europe. Quaternary Science Reviews 19, 1155–1231. https://doi.org/10.1016/S0277-3791(99)00034-7

Allen, J.R.L., 1997. Simulation models of salt-marsh morphodynamics: some implications for high-intertidal sediment couplets related to sea-level change. Sedimentary Geology 113, 211–223. https://doi.org/10.1016/S0037-0738(97)00101-2

Anisfeld, S.C., Tobin, M.J., Benoit, G., 1999. Sedimentation Rates in Flow-Restricted and Restored Salt Marshes in Long Island Sound. Estuaries 22, 231. https://doi.org/10.2307/1352980

Appleby, P.G., Oldfield, F., 1978. The calculation of lead-210 dates assuming a constant rate of supply of unsupported 210Pb to the sediment. Catena 5, 1–8.

Atwater, B., Hemphill-Haley, E., 1996. Preliminary Estimates of Recurrence Intervals for Great Earthquakes of the Past 3500 Years at Northeastern Willapa Bay, Washington (No. Open-File Report 96-001). U.S. Geological Survey.

Baranes, H.E., Woodruff, J.D., Geyer, W.R., Yellen, B.C. and Richardson, J.B., Sources, Mechanisms, and Timescales of Sediment Delivery to a New England Salt Marsh. Journal of Geophysical Research: Earth Surface, doi: 10.1029/2021JF006478.

Bertness, M.D., 1991. Zonation of Spartina Patens and Spartina Alterniflora in New England Salt Marsh. Ecology 72, 138–148. https://doi.org/10.2307/1938909

Boumans, R.M.J., Burdick, D.M., Dionne, M., 2002. Modeling Habitat Change in Salt Marshes After Tidal Restoration. Restoration Ecology 10, 543–555. https://doi.org/10.1046/j.1526-100X.2002.02032.x

Buynevich, I.V., Donnelly, J.P., 2006. Geological Signatures of Barrier Breaching and Overwash, Southern Massachusetts, USA. Journal of Coastal Research 112–116.

Cahoon, D.R., Lynch, J.C., Roman, C.T., Schmit, J.P., Skidds, D.E., 2019. Evaluating the Relationship Among Wetland Vertical Development, Elevation Capital, Sea-Level Rise, and Tidal Marsh Sustainability. Estuaries and Coasts 42, 1–15. https://doi.org/10.1007/s12237-018-0448-x

Chant, R.J., Ralston, D.K., Ganju, N.K., Pianca, C., Simonson, A.E., Cartwright, R.A., 2021. Sediment Budget Estimates for a Highly Impacted Embayment with Extensive Wetland Loss. Estuaries and Coasts 44, 608–626. https://doi.org/10.1007/s12237-020-00784-3

Croudace, I.W., Rindby, A., Rothwell, R.G., 2006. ITRAX: description and evaluation of a new multi-function X-ray core scanner. Geological Society, London, Special Publications 267, 51–63.

Cundy, A.B., Croudace, I.W., 1996. Sediment Accretion and Recent Sea-level Rise in the Solent, Southern England: Inferences from Radiometric and Geochemical Studies. Estuarine, Coastal and Shelf Science 43, 449–467. https://doi.org/10.1006/ecss.1996.0081

D'Alpaos, A., Lanzoni, S., Marani, M., Rinaldo, A., 2007. Landscape evolution in tidal embayments: Modeling the interplay of erosion, sedimentation, and vegetation dynamics. Journal of Geophysical Research: Earth Surface 112. https://doi.org/10.1029/2006JF000537

Day, J.W., Rybczyk, J., Scarton, F., Rismondo, A., Are, D., Cecconi, G., 1999. Soil Accretionary Dynamics, Sea-Level Rise and the Survival of Wetlands in Venice Lagoon: A Field and Modelling Approach. Estuarine, Coastal and Shelf Science 49, 607–628. https://doi.org/10.1006/ecss.1999.0522

Deegan, L.A., Johnson, D.S., Warren, R.S., Peterson, B.J., Fleeger, J.W., Fagherazzi, S., Wollheim, W.M., 2012. Coastal eutrophication as a driver of salt marsh loss. Nature 490, 388–392. https://doi.org/10.1038/nature11533

Emery, K.O., Wigley, R.L., Rubin, M., 1965. A Submerged Peat Deposit Off the Atlantic Coast of the United States1. Limnology and Oceanography 10, R97–R102. https://doi.org/10.4319/lo.1965.10.suppl2.r97

Fagherazzi, S., Furbish, D.J., 2001. On the shape and widening of salt marsh creeks. Journal of Geophysical Research: Oceans 106, 991–1003. https://doi.org/10.1029/1999JC000115

FitzGerald, D.M., 1988. Shoreline Erosional-Depositional Processes Associated with Tidal Inlets, in: Aubrey, D.G., Weishar, L. (Eds.), Hydrodynamics and Sediment Dynamics of Tidal Inlets, Lecture Notes on Coastal and Estuarine Studies. Springer, New York, NY, pp. 186–225. https://doi.org/10.1007/978-1-4757-4057-8_11

FitzGerald, D.M., Hughes, Z., 2019. Marsh Processes and Their Response to Climate Change and Sea-Level Rise. Annual Review of Earth and Planetary Sciences 47, 481–517. https://doi.org/10.1146/annurev-earth-082517-010255
Freitas, F., Ball, D., 1995. Warnings Ignored! The Story of The Portland Gale November, 1898. Converpage, Scituate Massachusetts.
French, J., 2006. Tidal marsh sedimentation and resilience to environmental change: Exploratory modelling of tidal, sea-level and sediment supply forcing in predominantly allochthonous systems. Marine Geology, Proceedings of the 6th International Congress on Tidal Sedimentology (Tidalites 2004) 235, 119–136. https://doi.org/10.1016/j.margeo.2006.10.009
Gannett, H., Grambs, W.J., 1888. Massachusetts - Duxbury Sheet. USGS Topographic Maps.
Green, G., 1838. On the motion of waves in a variable canal of small depth and width. Transactions of the Cambridge Philosophical Society 6, 457.
Hayes, M.O., 1979. Barrier island morphology as a function of tidal and wave regime. In: Leatherman SP (ed) Barrier Islands. Academic Press, New York 1, 27.
Holmquist, J.R., Windham-Myers, L., Bliss, N., Crooks, S., Morris, J.T., Megonigal, J.P., Troxler, T., Weller, D., Callaway, J., Drexler, J., Ferner, M.C., Gonneea, M.E., Kroeger, K.D., Schile-Beers, L., Woo, I., Buffington, K., Breithaupt, J., Boyd, B.M., Brown, L.N., Dix, N., Hice, L., Horton, B.P., MacDonald, G.M., Moyer, R.P., Reay, W., Shaw, T., Smith, E., Smoak, J.M., Sommerfield, C., Thorne, K., Velinsky, D., Watson, E., Grimes, K.W., Woodrey, M., 2018. Accuracy and Precision of Tidal Wetland Soil Carbon Mapping in the Conterminous United States. Scientific Reports 8, 9478. https://doi.org/10.1038/s41598-018-26948-7
Hopkinson, C.S., Morris, J.T., Fagherazzi, S., Wollheim, W.M., Raymond, P.A., 2018. Lateral Marsh Edge Erosion as a Source of Sediments for Vertical Marsh Accretion. Journal of Geophysical Research: Biogeosciences 123, 2444–2465. https://doi.org/10.1029/2017JG004358
Jay, D.A., 1991. Green's law revisited: Tidal long-wave propagation in channels with strong topography. Journal of Geophysical Research: Oceans 96, 20585–20598. https://doi.org/10.1029/91JC01633
Kirwan, M.L., Guntenspergen, G.R., 2010. Influence of tidal range on the stability of coastal marshland. Journal of Geophysical Research: Earth Surface 115. https://doi.org/10.1029/2009JF001400
Lambeck, K., Rouby, H., Purcell, A., Sun, Y., Sambridge, M., 2014. Sea level and global ice volumes from the Last Glacial Maximum to the Holocene. Proceedings of the National Academy of Sciences 111, 15296–15303. https://doi.org/10.1073/pnas.1411762111
Langston, A.K., Durán Vinent, O., Herbert, E.R., Kirwan, M.L., 2020. Modeling long-term salt marsh response to sea level rise in the sediment-deficient Plum Island Estuary, MA. Limnology and Oceanography 65, 2142–2157. https://doi.org/10.1002/lno.11444
Lanzoni, S., Seminara, G., 1998. On tide propagation in convergent estuaries. Journal of Geophysical Research: Oceans 103, 30793–30812. https://doi.org/10.1029/1998JC900015
Lucke, J.B., 1934. A Theory of Evolution of Lagoon Deposits on Shorelines of Emergence. The Journal of Geology. https://doi.org/10.1086/624214
MassGIS Data: 2019 Aerial Imagery, 2019.
Morris, J.T., 2007. Ecological engineering in intertidial saltmarshes. Hydrobiologia 577, 161–168. https://doi.org/10.1007/s10750-006-0425-4
Mudd, S.M., Howell, S.M., Morris, J.T., 2009. Impact of dynamic feedbacks between sedimentation, sea-level rise, and biomass production on near-surface marsh stratigraphy and carbon accumulation. Estuarine, Coastal and Shelf Science 82, 377–389. https://doi.org/10.1016/j.ecss.2009.01.028

Nixon, S., 1995. Metal Inputs to Narragansett Bay: A History and Assessment of Recent Conditions. Rhode Island Sea Grant, Narragansett, RI.
O'Keefe Suttles, J.A., Eagle, M.J., Mann, A.C., Spivak, A., Sanks, K., Daniel, R., Kroeger, K.D., 2021. Collection, analysis, and age-dating of sediment cores from natural and restored salt marshes on Cape Cod, Massachusetts, 2015-16. https://doi.org/10.5066/P9R154DY
Pederson, D.C., Peteet, D.M., Kurdyla, D., Guilderson, T., 2005. Medieval Warming, Little Ice Age, and European impact on the environment during the last millennium in the lower Hudson Valley, New York, USA. Quaternary Research 63, 238–249. https://doi.org/10.1016/j.yqres.2005.01.001
Peirce, B., Whiting, H.L., Tittman, O.H., 1870. Sketch of North River, Mass. U.S. Coast Survey.
Pennington, W., Tutin, T.G., Cambray, R.S., Fisher, E.M., 1973. Observations on lake sediments using fallout 137Cs as a tracer. Nature 242, 324.
Pomeroy, L., Darley, W.M., Dunn, E.L., Gallagher, E.B., Haines, E.B., Whitney, D.M., 1981. Primary Production, in: The Ecology of a Salt Marsh. Springer-Verlag, New York.
Ralston, D.K., Talke, S., Geyer, W.R., Al-Zubaidi, H.A.M., Sommerfield, C.K., 2019. Bigger Tides, Less Flooding: Effects of Dredging on Barotropic Dynamics in a Highly Modified Estuary. Journal of Geophysical Research: Oceans 124, 196–211. https://doi.org/10.1029/2018JC014313
Rampino, M.R., Sanders, J.E., 1980. Holocene transgression in South-central Long Island, New York. Journal of Sedimentary Research 50, 1063–1079. https://doi.org/10.1306/212F7B7B-2B24-11D7-8648000102C1865D
Redfield, A.C., 1972. Development of a New England salt marsh. Ecological monographs 42, 201–237.
Reed, D.J., 1990. The impact of sea-level rise on coastal salt marshes. Progress in Physical Geography 14, 465–481.
Roman, C.T., Peck, J.A., Allen, J.R., King, J.W., Appleby, P.G., 1997. Accretion of a New England (U.S.A.) Salt Marsh in Response to Inlet Migration, Storms, and Sea-level Rise. Estuarine, Coastal and Shelf Science 45, 717–727. https://doi.org/10.1006/ecss.1997.0236
Roner, M., D'Alpaos, A., Ghinassi, M., Marani, M., Silvestri, S., Franceschinis, E., Realdon, N., 2016. Spatial variation of salt-marsh organic and inorganic deposition and organic carbon accumulation: Inferences from the Venice lagoon, Italy. Advances in Water Resources, Ecogeomorphological feedbacks of water fluxes, sediment transport and vegetation dynamics in rivers and estuaries 93, 276–287. https://doi.org/10.1016/j.advwatres.2015.11.011
Scott, D.B., Medioli, F.S., 1980. Living vs. Total Foraminiferal Populations: Their Relative Usefulness in Paleoecology. Journal of Paleontology 54, 814–831.
Scott, D.S., Medioli, F.S., 1978. Vertical zonations of marsh foraminifera as accurate indicators of former sea-levels. Nature 272, 528–531. https://doi.org/10.1038/272528a0
Shennan, I., Long, A.J., Rutherford, M.M., Green, F.M., Innes, J.B., Lloyd, J.M., Zong, Y., Walker, K.J., 1996. Tidal marsh stratigraphy, sea-level change and large earthquakes, i: a 5000 year record in washington, U.S.A. Quaternary Science Reviews 15, 1023–1059. https://doi.org/10.1016/S0277-3791(96)00007-8
Snedden, G.A., Cretini, K., Patton, B., 2015. Inundation and salinity impacts to above- and belowground productivity in Spartina patens and Spartina alterniflora in the Mississippi River deltaic plain: Implications for using river diversions as restoration tools. Ecological Engineering 81, 133–139. https://doi.org/10.1016/j.ecoleng.2015.04.035
Talke, S.A., Kemp, A.C., Woodruff, J., 2018. Relative Sea Level, Tides, and Extreme Water Levels in Boston Harbor From 1825 to 2018. Journal of Geophysical Research: Oceans 123, 3895–3914. https://doi.org/10.1029/2017JC013645

Temmerman, S., Govers, G., Wartel, S., Meire, P., 2003. Spatial and temporal factors controlling short-term sedimentation in a salt and freshwater tidal marsh, Scheldt estuary, Belgium, SW Netherlands. Earth Surface Processes and Landforms 28, 739–755. https://doi.org/10.1002/esp.495

Tetra Tech EC, Inc., 2005. Comprehensive Site Assessment Report: Fireworks I.

Turner, R.E., Howes, B.L., Teal, J.M., Milan, C.S., Swenson, E.M., Tonerb, D.D.G.-, 2009. Salt marshes and eutrophication: An unsustainable outcome. Limnology and Oceanography 54, 1634–1642. https://doi.org/10.4319/lo.2009.54.5.1634

Watson, E.B., Oczkowski, A.J., Wigand, C., Hanson, A.R., Davey, E.W., Crosby, S.C., Johnson, R.L., Andrews, H.M., 2014. Nutrient enrichment and precipitation changes do not enhance resiliency of salt marshes to sea level rise in the Northeastern U.S. Climatic Change 125, 501–509. https://doi.org/10.1007/s10584-014-1189-x

Wolters, S., Zeiler, M., Bungenstock, F., 2010. Early Holocene environmental history of sunken landscapes: pollen, plant macrofossil and geochemical analyses from the Borkum Riffgrund, southern North Sea. Int J Earth Sci (Geol Rundsch) 99, 1707–1719. https://doi.org/10.1007/s00531-009-0477-6

Yellen, B., Woodruff, J., Ladlow, C., Ralston, D.K., Fernald, S., Lau, W., 2021. Rapid tidal marsh development in anthropogenic backwaters. Earth Surface Processes and Landforms 46, 554–572. https://doi.org/10.1002/esp.5045

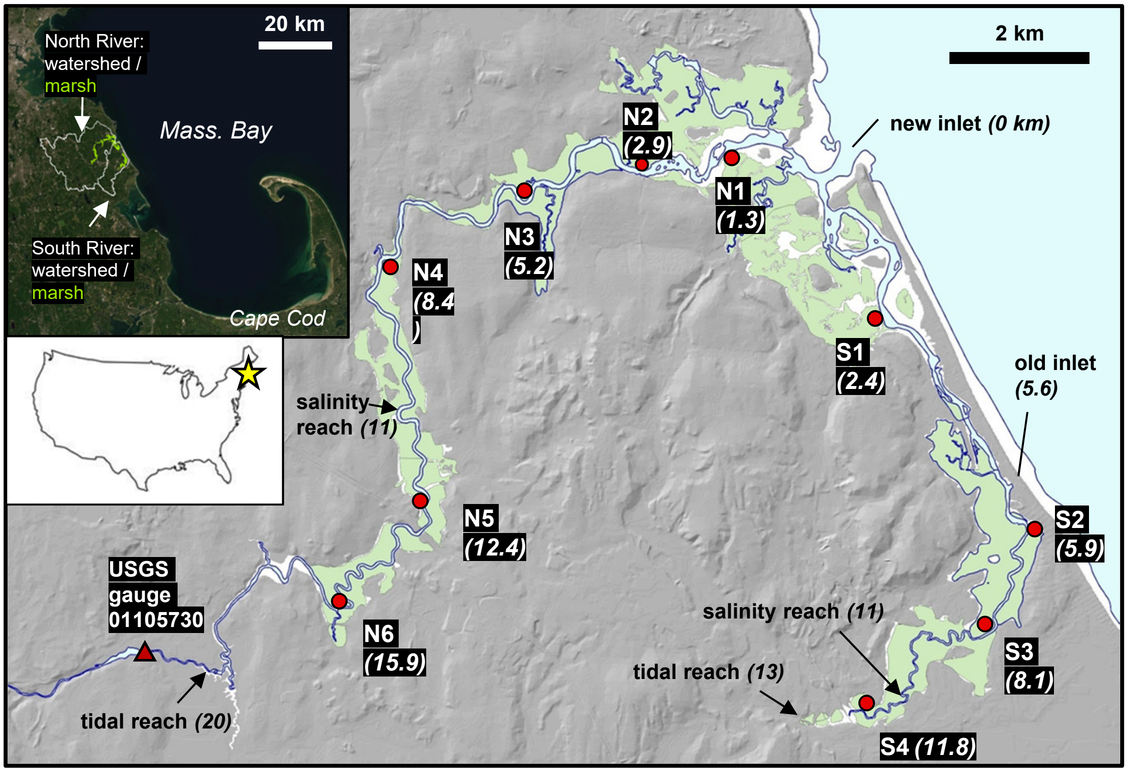

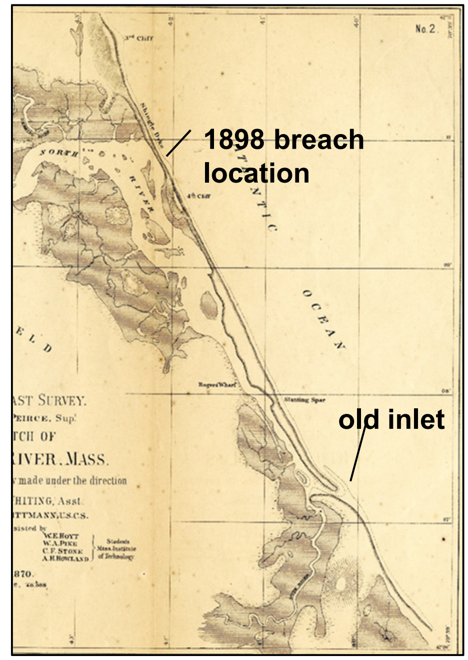

Figure 1: Site map of the North-South Rivers Estuary (NSRE). Red dots correspond to core transect and water level observation locations; numbers in parentheses refer to river distance to the inlet in km. Marsh area (National Wetlands Inventory, 2013) is depicted with green, intertidal areas in white, and upland is shaded in grey. The panel at right shows the North South Rivers Estuary barrier beach as depicted in an 1870 chart (Pierce et al., 1870).

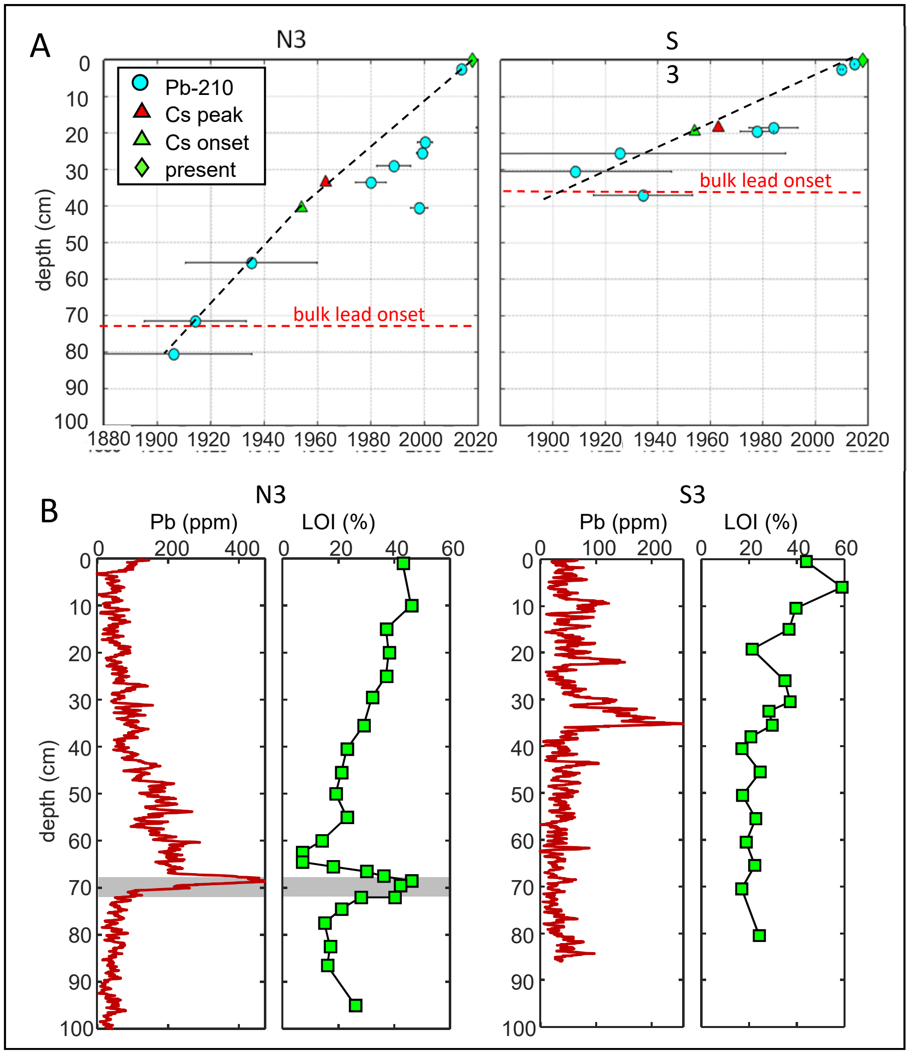

Figure 2: Panel A: Age versus depth models from representative cores ar N3 and S3, including age controls derived from ^{210}Pb, ^{137}Cs onset and peak, and coring date in 2018. Panel B: Lead and LOI profiles from North River and South River representative cores. Lead profiles from ITRAX scanner in units of ppm based on an empirical regression presented in Baranes et al. (2022). Grey shaded bars in N3 profiles depict the depth of the visually identifiable marker horizon.

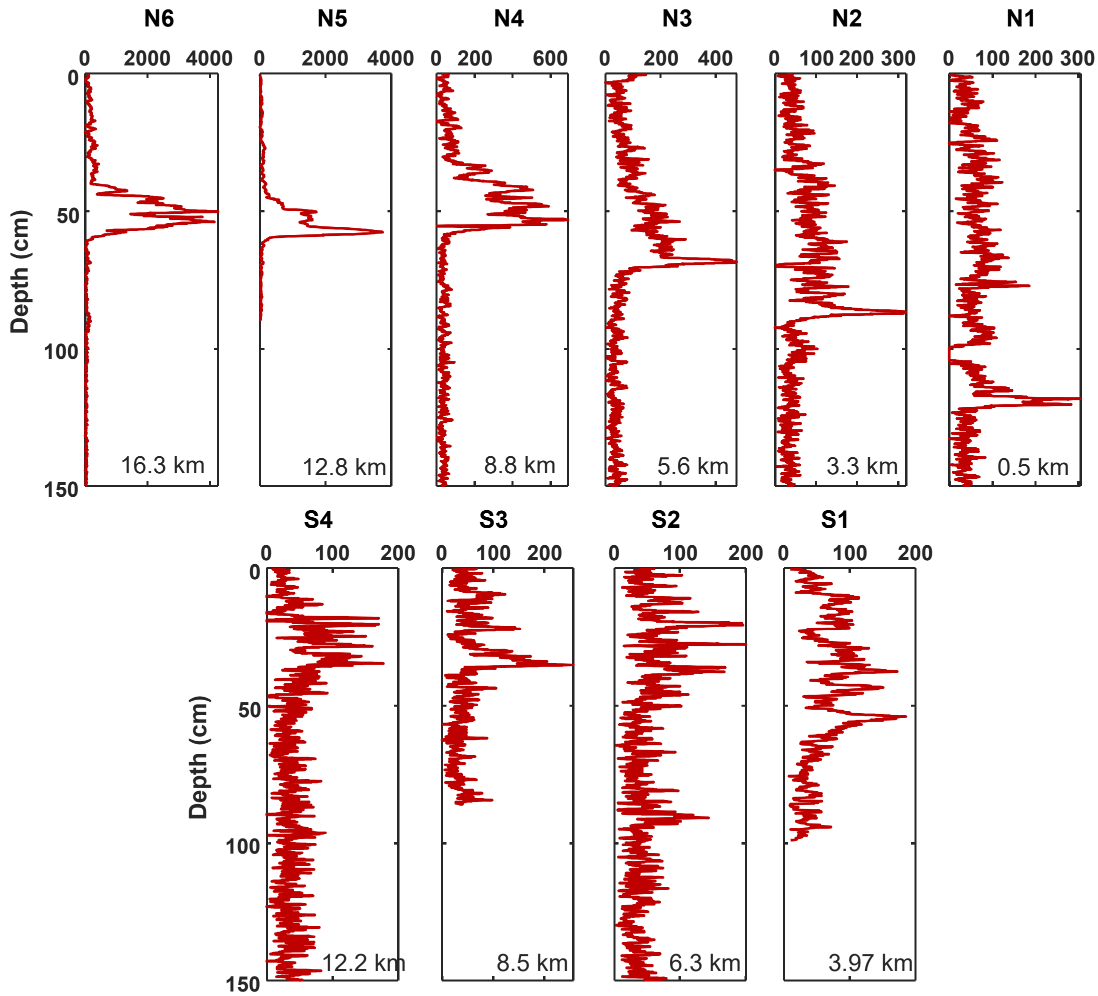

Figure 3 Lead profiles from representative sediment cores from the North River (top row) and South River (bottom row) from ITRAX XRF corescanner data converted to parts per million according to a site-specific empirical regression reported in Baranes et al. (2022) where $PPM_{Pb}=1.14*Counts_{xrf}-0.48$. River distance from the shared NSRE inlet is shown at the bottom of each panel.

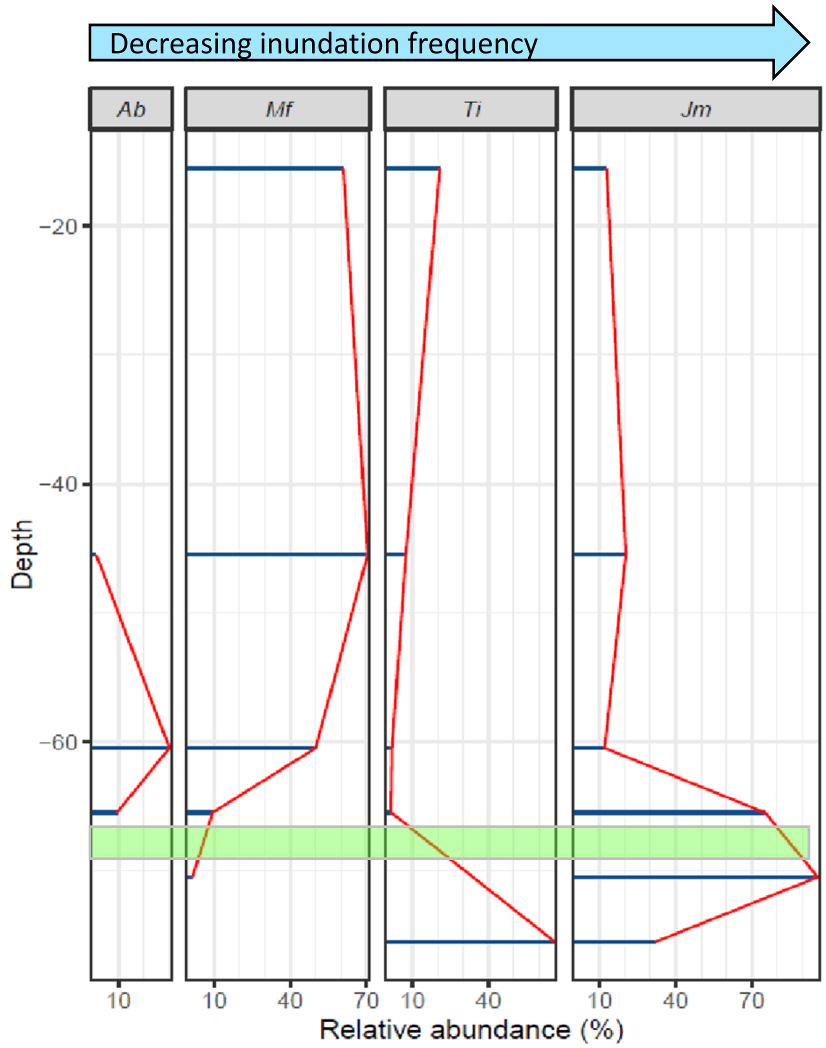

Figure 4 - Total abundances of foraminifera taxa by percent in five discrete 1 cm sediment samples (see section 4.3), including *Jadammina macrescens (Jm), Trochammina inflata (Ti), Miliammina fusca (Mf), Ammobaculites (Ab)*. Taxa are ordered from left to right according to the species elevation optima from Wright et al (2011) with less frequent inundation on the left. The green shaded depth indicates the depth of the cohesive organic horizon.

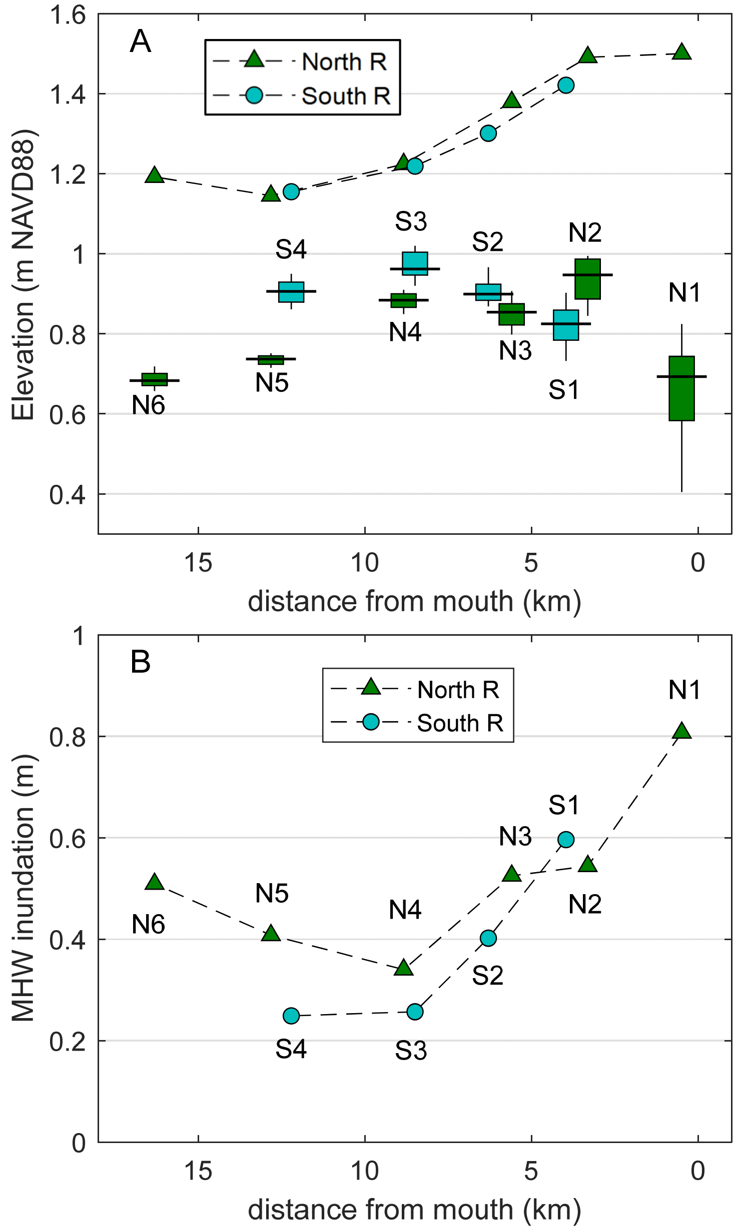

Figure 5 – Mean high water (MHW) and marsh platform elevation summary along the North and South Rivers relative to the NAVD88 vertical datum. Panel A shows MHW at marsh transect locations (see Fig. 1) and summaries of RTK-derived marsh platform elevations at each transect location depicted. Boxes represent the 25th-75th centiles, and whiskers representing the 10th and 90th centiles. Panel B shows the average marsh inundation depth at each transect calculated as the MHW minus the median marsh platform elevation. Data labels (N1 etc) correspond to locations depicted in Fig. 1.

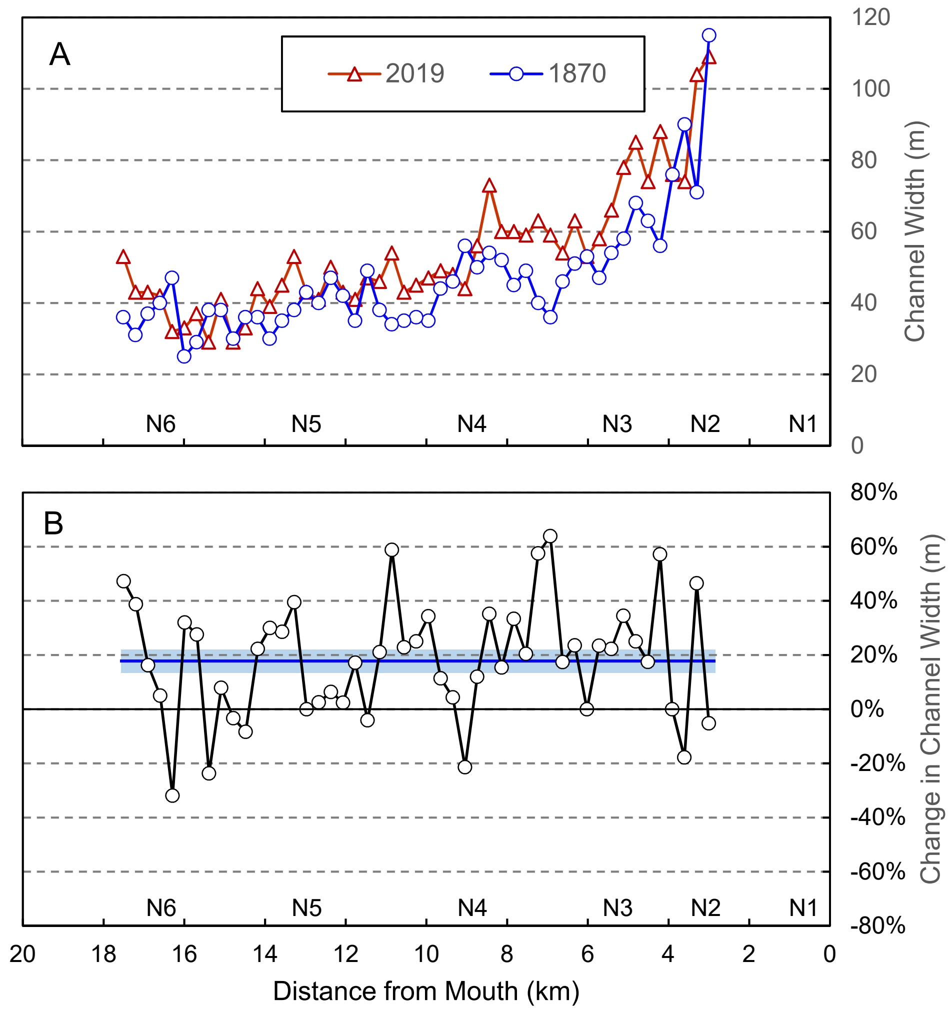

Figure 6 – Panel A shows North River channel widths in 2019 and 1870. Panel B shows the percentage change in North River width from 1870 to 2019. Negative % values indicate narrowing, and positive % values indicate widening. The blue line represents the average channel widening. The shaded area represents the standard error.

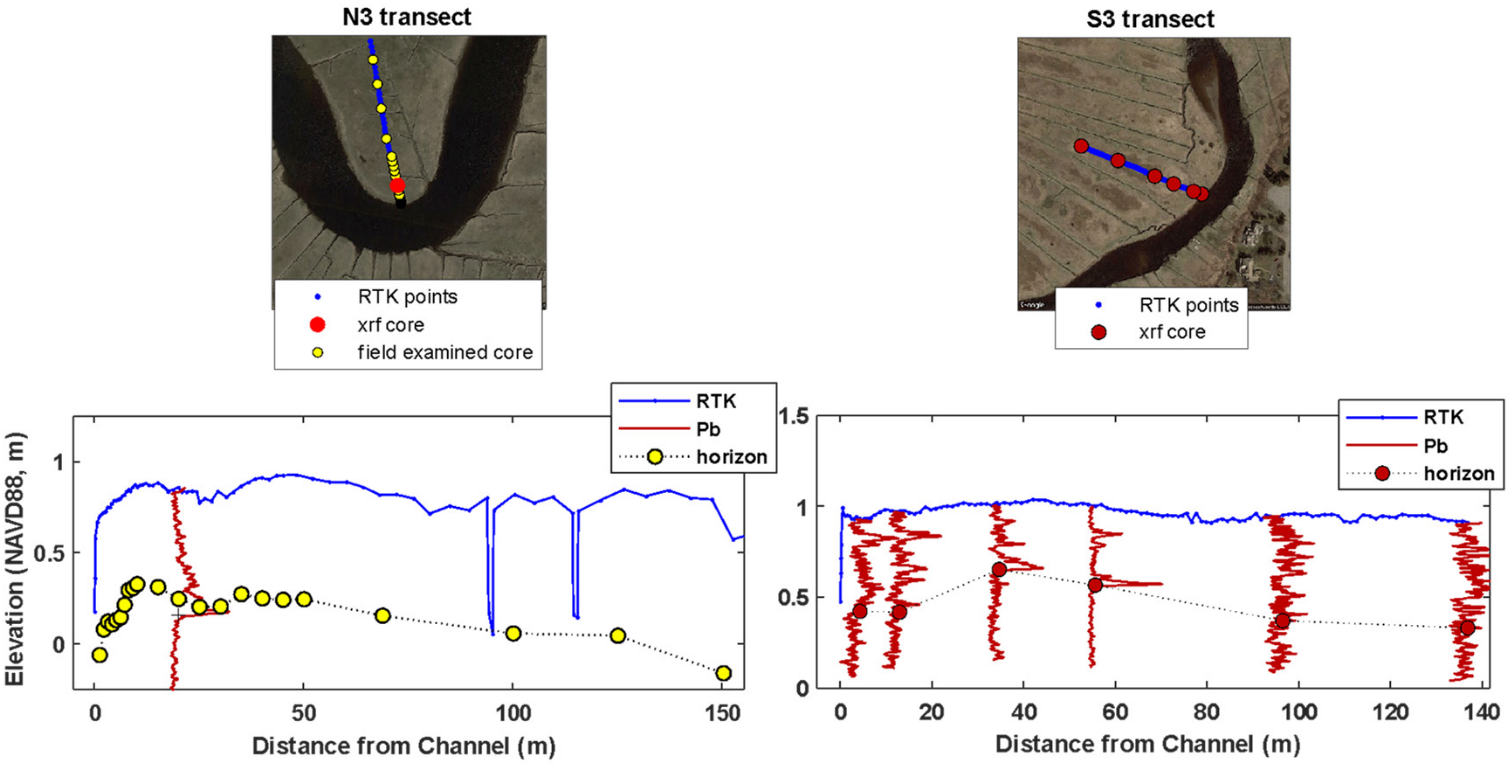

Supplementary Figure 1: Elevation and depth to chronostratigraphic tie points for sediment core transects N3 and S3. The upper-left panel shows the location of the sediment cores scanned via XRF spectroscopy for lead abundance (red dots) and locations of cores that were inspected visually in the field with the depth of cohesive, organic-rich layer noted (yellow dots). Arrows indicate the location of cores selected for gamma spectroscopy. The lower left panel shows an elevation profile from the marsh surface RTK points (blue dots) with elevation of the marker horizon (yellow dots) and the lead profile from core N3C1. The right panels show similar observations for South River transect S3. Because the organic marker horizon was not present in the South River marsh, lead profiles for cores away from the channel are shown to illustrate the continuity in deposition rates away from the channel.